Direct observation of the lattice precursor of the metal-to-insulator transition in V2O3 thin films by surface acoustic waves

J. Kündel, P. Pontiller, C. Müller, Günter Obermeier, Z. Liu, A. A. Nateprov, Andreas Hörner, Achim Wixforth, Siegfried R. Horn, Reinhard Tidecks

Angaben zur Veröffentlichung / Publication details:

Kündel, J., P. Pontiller, C. Müller, Günter Obermeier, Z. Liu, A. A. Nateprov, Andreas Hörner, Achim Wixforth, Siegfried R. Horn, and Reinhard Tidecks. 2013. "Direct observation of the lattice precursor of the metal-to-insulator transition in V2O3 thin films by surface acoustic waves." Applied Physics Letters 102 (10): 101904. https://doi.org/10.1063/1.4794948.

Applied Physics Letters

Direct observation of the lattice precursor of the metal-to-insulator transition in V_2O_3 thin films by surface acoustic waves

Cite as: Appl. Phys. Lett. **102**, 101904 (2013); https://doi.org/10.1063/1.4794948
Submitted: 19 October 2012 • Accepted: 26 February 2013 • Published Online: 13 March 2013

J. Kündel, P. Pontiller, C. Müller, et al.

Direct observation of the lattice precursor of the metal-to-insulator transition in V_2O_3 thin films by surface acoustic waves

J. Kündel, P. Pontiller,[a] C. Müller,[b] G. Obermeier, Z. Liu, A. A. Nateprov, A. Hörner, A. Wixforth, S. Horn, and R. Tidecks
Institut für Physik der Universität Augsburg, Universitätsstrasse 1, D-86159 Augsburg, Germany

(Received 19 October 2012; accepted 26 February 2013; published online 13 March 2013)

A surface acoustic wave (SAW) delay line is used to study the metal-to-insulator (MI) transition of V_2O_3 thin films deposited on a piezoelectric $LiNbO_3$ substrate. Effects contributing to the sound velocity shift of the SAW which are caused by elastic properties of the lattice of the V_2O_3 films when changing the temperature are separated from those originating from the electrical conductivity. For this purpose the electric field accompanying the elastic wave of the SAW has been shielded by growing the V_2O_3 film on a thin metallic Cr interlayer (coated with Cr_2O_3), covering the piezoelectric substrate. Thus, the recently discovered lattice precursor of the MI transition can be directly observed in the experiments, and its fine structure can be investigated. [http://dx.doi.org/10.1063/1.4794948]

The metal-to-insulator (MI) transition, occurring in the vanadium oxide V_2O_3,[1,2] is usually interpreted by regarding the compound as a Mott-Hubbard system.[3–10] However, together with the electrical transition a structural change occurs.[11] This is the reason why there is no complete understanding of the transition although it is already extensively investigated.[12–17]

Recently, light was shed on the role of the lattice at the MI transition of V_2O_3 in the paramagnetic metallic region. A precursor of the transition was found by extended X-ray absorption fine structure measurements.[18,19] Detailed investigations by surface acoustic waves (SAW) of V_2O_3 thin films, deposited on piezoelectric substrates, confirm the existence of this precursor and suggest that it arises from the lattice.[20–22] Moreover, oscillations of the sound velocity of the SAW with steep reductions were observed during the MI transition.[21] Possibly this phenomenon is an evidence for the sound velocity anomaly, recently predicted by the compressive Hubbard model.[23]

Meanwhile, the existence of the precursor has been established by Brillouin scattering.[24] Furthermore lattice softening effects were observed in the vicinity of the critical point of Cr-doped V_2O_3 by sound velocity measurements as a function of pressure with the temperature as a parameter.[25]

In the SAW experiments the lattice precursor was first detected by its influence on the sound velocity shift.[20] Then, with a special high sensitive measuring technique also its action on the attenuation could be observed.[21]

To get knowledge about the contribution of the lattice precursor in the V_2O_3 films on the sound velocity shift of the SAW, when decreasing the temperature, we so far calculated the part caused by a change of the conductivity of the film and compared it with the experiments. The remaining sound velocity shift, which could not be explained by conductivity changes, was then attributed to the lattice precursor.[20]

This method is, however, somewhat indirect and depends on the model used to describe the sound velocity shift caused by conductivity changes in the V_2O_3 film. Therefore, we developed a sample design, where the electric field accompanying the elastic wave of the SAW is shielded by a metallic Cr interlayer. Thus, only the elastic wave couples to the V_2O_3 film.

The SAW device, sketched in Fig. 1, and the measuring method are similar to those used in our preceding work.[20,21] Again, a 128° rotated YX cut of $LiNbO_3$ was used as a piezoelectric substrate. To emit and receive the SAW, two interdigital transducers (IDTs) were placed on the substrate, separated by a sound path of $L_{SP} = 2.654$ mm. Each IDT consists of 10 pairs of fingers in the split 2 design (height of gold 50 nm on 5 nm Ti undercoating) fabricated by lithographic methods. From the spacing of the finger electrodes results a wave length of the SAW of $\lambda = 48\ \mu$m.

The metallic Cr film was deposited directly on the sound path of the $LiNbO_3$ substrate by electron beam evaporation (thickness 25 nm, measured by a quartz microbalance during deposition).

The surface of this film was coated by its electrically insulating oxide, Cr_2O_3, grown by exposing the film to air at room temperature.

Since V_2O_3 has a similar structure (describing the lattice as distorted hexagonal[26]) and lattice parameters as Cr_2O_3 at room temperature,[11,27,28] good growth conditions are expected for V_2O_3 films on top of Cr_2O_3.[28–30] The thickness of the Cr_2O_3 surface layer is expected to be of order 1 nm.[31]

Next, the V_2O_3 film was deposited on the oxidized Cr layer by electron beam evaporation from a sintered V_2O_3 powder target and subsequently tempered in a reducing Ar/H_2 atmosphere.[32] The thickness of the V_2O_3 film was 300 nm (measured ex situ with a Dektak contact profilometer of Veeco Instruments, employing a diamond-tipped stylus).

The growth of V_2O_3 deposited on a Cr/Cr_2O_3 layer covering a $LiNbO_3$ substrate was in detail investigated in

[a]Present address: Universität Bayreuth, Fakultät für Angewandte Naturwissenschaften, Lehrstuhl für Werkstoffverarbeitung, Universitätsstrasse 30, D-95447 Bayreuth, Germany.
[b]Author to whom correspondence should be addressed. Electronic mail: claus.mueller@physik.uni-augsburg.de. Tel.: +49 (0) 821/598/2111. Fax: +49 (0) 821/598/3411.

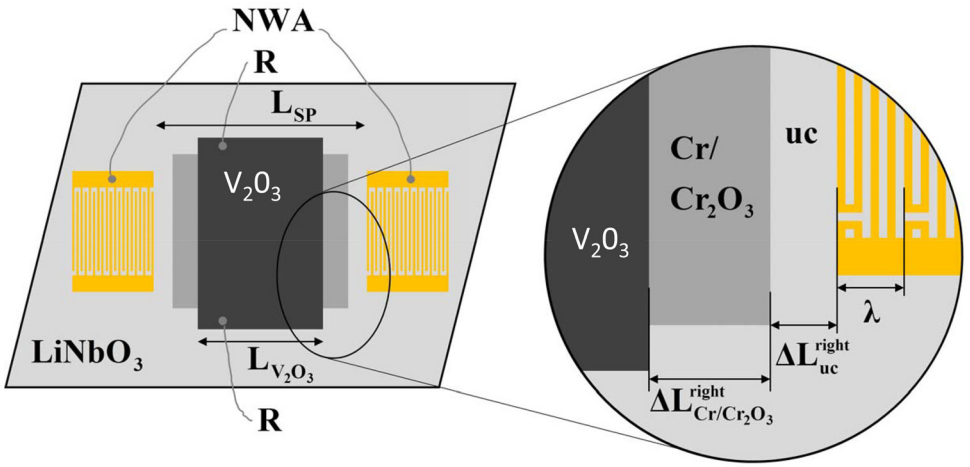

FIG. 1. Sketch of the SAW transmission delay line with two IDTs on top of a $LiNbO_3$ substrate. The V_2O_3 film to be investigated is grown on top of a Cr/Cr_2O_3 layer, which is directly deposited on the $LiNbO_3$ substrate. The length of the sound path between the IDTs is $L_{SP} = 2.654$ mm, the length of the V_2O_3 film is $L_{V2O3} = 2.233$ mm, the total length of the Cr/Cr_2O_3 layer extending the V_2O_3 layer is $\Delta L_{Cr/Cr2O3} = (53\,\mu m + 92\,\mu m)$ on the left and right side, respectively. The length of the uncovered sound path $\Delta L_{uc} = (3\,\mu m + 274\,\mu m)$ for left and right, respectively. The dimension of one IDT is $L_{IDT} = 474\,\mu m$, and the propagation length of the SAW therein is 334 μm. All geometrical distances were determined by a scanning electron microscope.

Refs. 33 and 34, including the problem of electron tunneling through the Cr_2O_3 barrier. The dc resistance measurements of the MI transition shown below indicate no appreciable leak currents.

The dc resistance measurements were performed using a two point method, applying a constant voltage of 0.1 V. The SAW measurements were carried out using a vector network analyzer (NWA). The measuring method is described in detail in Ref. 20. The center frequency was 81 MHz with a measuring span of 50 MHz. The measurements were carried out in a cryostat containing a variable temperature insert (VTI), allowing temperatures between room temperature and 4.2 K.

Such SAW measurements were performed in Ref. 34. However, to get the temperature dependent sound velocity, $v_{V2O3}(T)$, of the SAW from the propagation time during which the SAW passes the V_2O_3 covered region L_{V2O3} (see Fig. 1), this propagation time has to be extracted from the total measured time. In our previous works,[20,21] dealing with a V_2O_3 film directly deposited on the $LiNbO_3$ substrate in a certain range of the sound path, this was simply done by subtracting the length of the film from the effective distance of the IDTs and reducing the total propagation time of the SAW by the time obtained by dividing this difference by the room temperature sound velocity of $LiNbO_3$. The effective distance of the IDTs was determined from the propagation time of the SAW, traveling from IDT to IDT, for the uncovered case and the room temperature sound velocity of $LiNbO_3$. In the present work, a more detailed procedure is necessary, considering the different sections of the sound path.

Therefore, we had to calculate the propagation times for the propagation areas ΔL_{IDT}, ΔL_{UC}, $\Delta L_{Cr/Cr2O3}$, and L_{V2O3}, utilizing successively more complex layered, but in principal identical SAW devices. Here, ΔL_{IDT} is not the geometrical dimension of the IDT, but the effective length, which the SAW propagates into both IDT regions. Moreover, ΔL_{UC} is the total uncovered region, and $\Delta L_{Cr/Cr2O3}$ is the Cr/Cr_2O_3 covered region that exceeds the V_2O_3 film, i.e., which is non-covered with V_2O_3 (see Fig. 1).

First, to get ΔL_{IDT} we used an identical SAW device with an uncovered sound path, i.e., $\Delta L_{UC} = L_{SP}$. The propagation time of the SAW along ΔL_{UC} at room temperature can be calculated using the literature value for the sound velocity v_{UC} at room temperature ($v_{0,RT} = 3978.2$ m/s of a SAW on a 128° rot YX $LiNbO_3$ substrate[35]). The difference of the measured total propagation time at room temperature (RT) and the calculated propagation time along the uncovered sound path yields the time t_{IDT} which the SAW travels into the transducers. Then $\Delta L_{IDT} = v_{IDT}\, t_{IDT}$. Here v_{IDT} is so far unknown. It can however be calculated. Considering that the IDT region is 50% metalized, i.e., short circuited (SC), it is $t_{IDT} = t_0 + t_{sc}$ with $t_0 = \Delta L_{IDT}/2v_{0,RT}$ and $t_{sc} = \Delta L_{IDT}/2v_{sc,RT}$. With $v_{IDT} = \Delta L_{IDT}/t_{IDT}$ the velocity along the IDT regions is then $v_{IDT} = 2v_{0,RT}\, v_{sc,RT}/(v_{0,RT} + v_{sc,RT})$.

The short circuited sound velocity v_{sc} can be calculated via the relation $v_{sc} = v_0(1\text{-}K^2/2)$ with $K^2 = 0.056$ the electromechanical coupling constant.[20] Thus, ΔL_{IDT} could be obtained with this device and then taken constant for all other devices and measurements, performed as function of temperature. Then $t_{IDT} = \Delta L_{IDT}/v_{IDT}$ with $v_{IDT} = 2v_0(T)\, v_{sc}(T)/(v_0(T) + v_{sc}(T))$, where $v_{sc}(T) = v_0(T)(1\text{-}K^2/2)$ with $K^2 = 0.056$ for all temperatures.

To verify the last relation for $v_{sc}(T)$, the measured velocity $v_0(T)$ of an uncovered $LiNbO_3$ substrate was used to determine the short circuited sound velocity $v_{sc}(T)$ via the relation $v_{sc}(T) = v_0(T)(1\text{-}K^2/2)$ with $K^2 = 0.056$ the electromechanical coupling constant.[20] The latter we found nearly temperature independent, when comparing the velocity $v_{sc}(T)$ with the velocity $v_{Cr/Cr2O3}(T)$ of a Cr-metalized SAW device. Due to the short-circuiting of the surface, in first approximation the measured $v_{Cr/Cr2O3}(T)$ is equal to the thus calculated $v_{sc}(T)$. This enables us to determine the temperature dependent propagation times t_{UC} and $t_{Cr/Cr2O3}$ for a given geometry via $v_0(T)$ and $v_{sc}(T)$, respectively.

Hereby $v_{Cr/Cr2O3}(T)$ was obtained from a Cr/Cr_2O_3 device, which consists of three regions, $L_{eff} = \Delta L_{IDT} + \Delta L_{UC} + \Delta L_{Cr/Cr2O3}$, by calculating the components of the total

measured propagation time $t_{total} = t_{IDT} + t_{UC} + t_{Cr/Cr2O3}$ with the known velocities $v_{UC}(T) = v_0(T)$ and v_{IDT}.

To yield the sound velocity $v_{V2O3}(T)$ the procedure was applied for a SAW device covered with a V_2O_3 film on top of a Cr/Cr_2O_3 interlayer, consisting of four different propagation areas $L_{eff} = \Delta L_{IDT} + \Delta L_{UC} + \Delta L_{Cr/Cr2O3} + L_{V2O3}$.

Now the relative sound velocity shift $\Delta v/v_0(T) = [v_{V2O3}(T)\text{-}v_{sc}(T) + x]/v_0(T)$ can be determined. Here, $v_0(T)$ is the sound velocity measured for uncovered $LiNbO_3$, $v_{sc}(T)$ is the short-circuited velocity that equates to $v_{Cr/Cr2O3}(T)$ for devices with a Cr/Cr_2O_3 interlayer. The variable x in the sum for Δv is temperature independent. It contains other effects, which are assumed to be constant, like the mass loading shift. Its value was set to adjust the relative sound velocity shift at room temperature to zero. The value of x differs slightly for warming and cooling measurements, which could be due to cycling effects or temperature shifts between specimen and temperature sensor, which is not directly placed at the sample.

In Fig. 2(a) the temperature dependence of the resistance is shown for a V_2O_3 film grown directly on $LiNbO_3$ whereas in Fig. 2(b) the V_2O_3 film was grown on a Cr/Cr_2O_3 sublayer. In both cases the jump of the resistance at the MI transition amounts to at least seven orders of magnitude. As typical for thin films, the transition temperature is suppressed below the bulk material value 170 K [Ref. 17], and a wider hysteresis is observed between cooling and warming.[20,21] Since in both samples the resistance increases to nearly the same value, there are no appreciable leak currents through the Cr film due to tunneling of electrons through the Cr_2O_3 layer. The inset shows the derivatives of the lg(R(T)) curves calculated after a linear interpolation of neighbouring data points and a smoothing procedure, to avoid artificial jumps in the derivative. The minima of the derivatives indicate the points of maximum absolute value of slope of the curves, which was considered as the temperature of the metal-to-insulator transition.

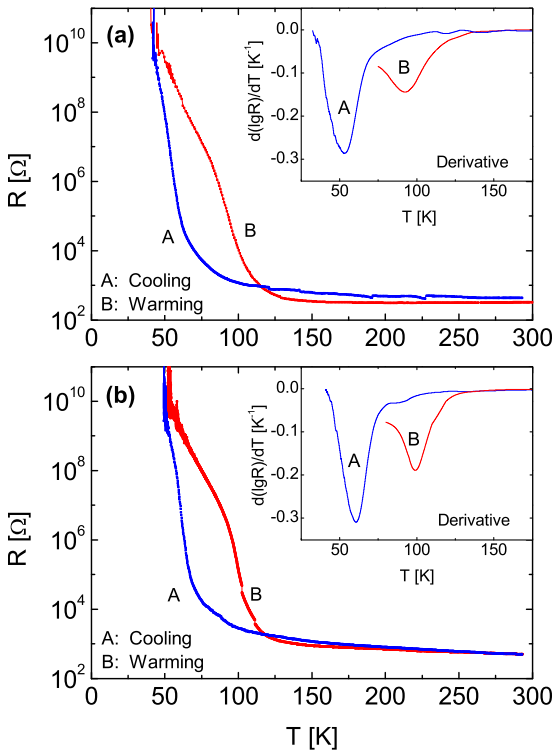

FIG. 2. Resistance, R, as a function of temperature, T, for a V_2O_3 film. The inset shows the derivative of the curve. (a) V_2O_3 grown directly on a $LiNbO_3$ substrate. (b) V_2O_3 grown on a Cr/Cr_2O_3 layer sublayer coating the $LiNbO_3$ substrate.

The sound velocity shift for the V_2O_3 film directly deposited on $LiNbO_3$ is plotted in Fig. 3. Caused by the change of the conductance of the V_2O_3 film, the normalized sound velocity shift $\Delta v/v_0(T) = [v_{V2O3}(T)\text{-}v_{sc}(T) + x]/v_0(T)$, with $x = 46$ m/s and 49.1 m/s for warming and cooling, respectively, shows a steep step-like change of about $0.028 = 2.8\%$, which is expected from the theory as discussed in detail in Ref. 20. Within the transition, two of the oscillations mentioned above and discussed in detail in Ref. 21 can be observed. As in our former work[21] these are more pronounced in the warm-up measurement.

The inset shows the lower part of the curves in higher magnification. The decrease of the sound velocity shift before its steep rise at the MI transition was interpreted in Refs. 20 and 21 as caused by a lattice precursor. However, in the present work much more details in the structure are visible. Describing the behavior upon cooling, the first deviation from the room temperature value occurs at about 250 K. Around 200 K a first minimum M1 appears, leading to a broad maximum at about 163 K. The main precursor structure is the second minimum M2 appearing below 150 K. The lowest value of M2 is reached at 100 K. The end of the seen precursor is a steep step of the sound velocity shift at the MI transition. Due to the temperature hysteresis the end of the seen precursor occurs at 91 K and 58 K for cooling and warming, respectively, i.e., the seen precursor for cooling is 33 K broader than for warming. The further development of this precursor structure or "signature of the lattice" is then masked by the sound velocity shift caused by the change of the conductance.

In Figs. 4(a) and 4(b) the range of the precursor is plotted together with a derivative of the dc resistance separately for cooling and warming, respectively. Although the main minimum of the precursor is more expressed for cooling, the overall structure is deeper and more expressed for warming.

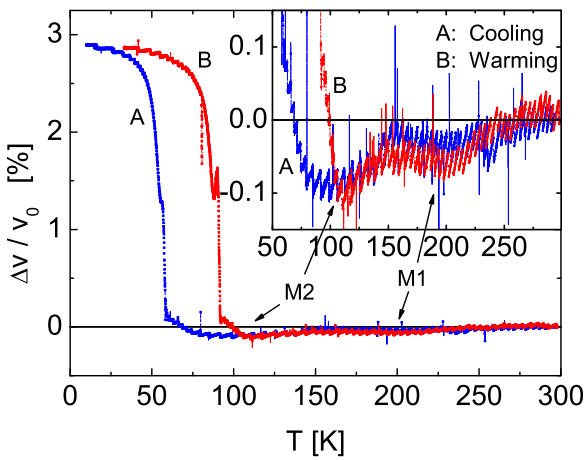

FIG. 3. Normalized sound velocity shift vs. temperature: $\Delta v/v_0(T) = [v_{V2O3}\text{-}v_{sc}(T) + x]/v_0(T)$. The V_2O_3 film was directly deposited on the $LiNbO_3$ substrate (cooling-warming cycle). Here $x = 49.1$ m/s and $x = 46$ m/s for cooling and warming, respectively. The inset shows the "precursor region" in higher magnification.

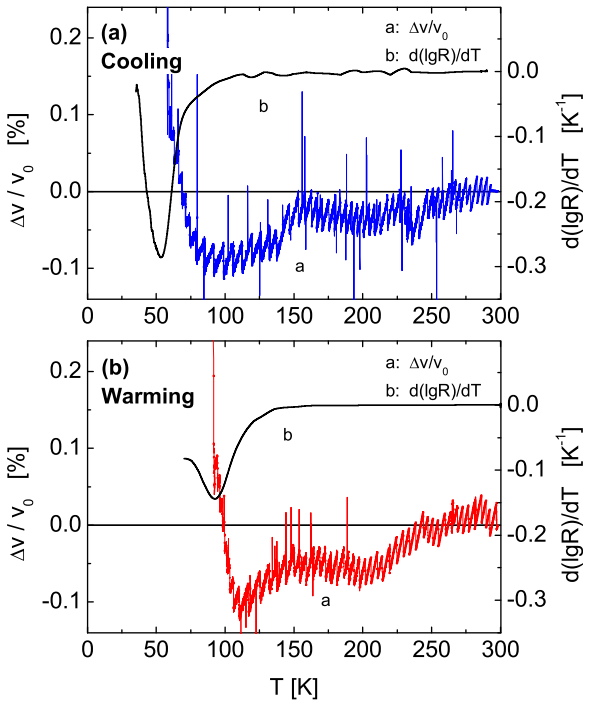

FIG. 4. Magnified representation of the normalized sound velocity shift vs. temperature: $\Delta v/v_0(T) = [v_{V2O3}\text{-}v_{sc}(T) + x]/v_0(T)$. The V_2O_3 film was directly deposited on the $LiNbO_3$ substrate. (a) Cooling, x = 49.1 m/s, (b) warming, x = 46 m/s. In addition the derivative of the lg(R(T)) curve of the V_2O_3 film is plotted.

In Figs. 5(a) and 5(b) the sound velocity shift $\Delta v/v_0(T) = [v_{V2O3}(T)\text{-}v_{sc}(T) + x]/v_0(T)$ observed for a V_2O_3 film grown on a Cr/Cr_2O_3 layer shielding the electric field of the SAW is shown. Here x = 3.1 m/s for warming and cooling. The absence of the steep increase of the sound velocity shift at the MI transition due to the change of the conductance of the V_2O_3 film indicates that only the elastic part of the SAW interacts with the V_2O_3 film.

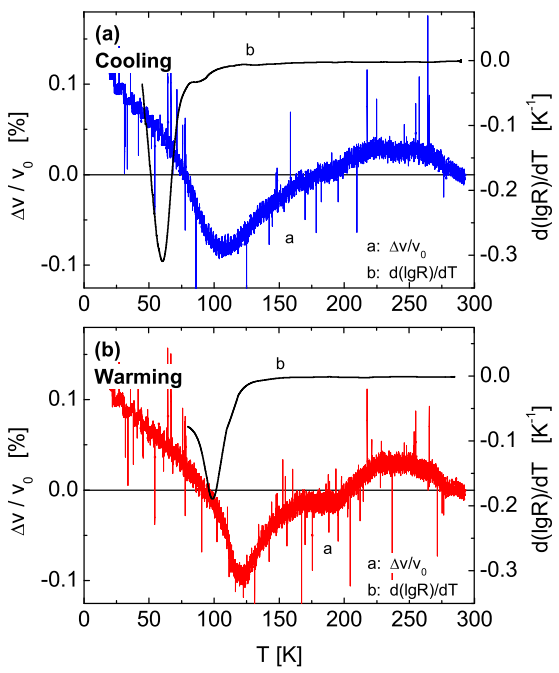

FIG. 5. Normalized sound velocity shift vs. temperature: $\Delta v/v_0(T) = [v_{V2O3}\text{-}v_{sc}(T) + x]/v_0(T)$ for a V_2O_3 film grown on a Cr/Cr_2O_3 layer, deposited on the $LiNbO_3$ substrate, shielding the electric wave of the SAW. (a) Cooling, x = 3.1 m/s, (b) warming, x = 3.1 m/s. In addition the derivative of the lg(R(T)) curve of the V_2O_3 film is plotted.

Describing the sound velocity shift upon cooling, the precursor structure is somewhat different from that one observed in the unshielded case. The main difference is that the sound velocity shift first increases and then decreases towards a minimum. As in the unshielded case this minimum is situated at the border of the MI transition, indicated by the beginning of the steep decrease of the derivative of the resistance of the V_2O_3 film. The sound velocity shift at the minimum (−0.08% for cooling, −0.1% for warming) is the same as in the unshielded case. Then, however, the sound velocity crosses continuously the MI transition region, exhibiting a change of slope (i.e., a flattening toward a linear behavior) at the temperature of the minimum of the derivative of the resistance curve, where the steepest part of the resistive transition occurs. The most remarkable result is that the sound velocity shift then increases to a positive value (+0.12% for cooling and warming) which has the same absolute value as observed in the minimum of the precursor structure. This indicates that there is an elastic distortion of the lattice at the beginning of the MI transition, which is of the same size as at the end of the transition.

Thus, one may conclude that on a scale of elastic effects the precursor structure of the sound velocity shift is not a small signature, as originally thought, but may possibly give evidence for a considerable driving force of the MI transition.

The authors want to thank R. Langer to be of assistance in preparing the present style of the figures. The present work was supported by SFB 484.

[1]M. Foëx, "Etude dilatométrique et électrique de l'ánomalie, présentée à basse température, par les sesquioxyde de vanadium," C. R. Acad. Sci. **223**, 1126 (1946).
[2]J. F. Morin, "Oxides which show a metal-to-insulator transition at the Neel temperature," Phys. Rev. Lett. **3**, 34 (1959).
[3]N. F. Mott, "Metal-insulator transition," Rev. Mod. Phys. **40**, 677 (1968).
[4]D. B. McWhan, T. M. Rice, and J. P. Remeika, "Mott transition in Cr-doped V_2O_3," Phys. Rev. Lett. **23**, 1384 (1969).
[5]M. Imada, A. Fujimori, and Y. Tokura, "Metal-insulator transitions," Rev. Mod. Phys. **70**, 1039 (1998).
[6]K. Held, G. Keller, V. Eyert, D. Vollhardt, and V. I. Anisimov, "Mott-Hubbard metal-insulator transition in paramagnetic V_2O_3: An LDA+DMFT(QMC) study," Phys. Rev. Lett. **86**, 5345 (2001).
[7]G. Keller, K. Held, V. Eyert, D. Vollhardt, and V. I. Anisimov, "Electronic structure of paramagnetic V_2O_3: Strongly correlated metallic and Mott insulating phase," Phys. Rev. B **70**, 205116 (2004).
[8]G. Kotliar and D. Vollhardt, "Strongly correlated materials: Insights from dynamical mean-field theory," Phys. Today **57**, 53 (2004).
[9]K. Held, I. A. Nekrasov, G. Keller, V. Eyert, N. Blümer, A. K. McMahan, R. T. Scalattar, Th. Pruschke, V. I. Anisimov, and D. Vollhardt, "Realistic investigations of correlated electron systems with LDA+DMFT," Phys. Status Solidi B **243**, 2599 (2006).
[10]D. Vollhardt, "Dynamical mean-field theory of electronic correlations in models and materials," AIP Conf. **1297**, 339 (2010).
[11]D. B. McWhan, A. Menth, J. P. Remeika, W. F. Brinkmann, and T. M. Rice, "Metal-insulator transitions in pure and doped V_2O_3," Phys. Rev. B **7**, 1920 (1973).
[12]E. Goering, M. Schramme, O. Müller, R. Barth, H. Paulin, M. Klemm, M. L. den Boer, and S. Horn, "LEED and photoemission study of the stability of VO_2 surfaces," Phys. Rev. B **55**, 4225 (1997).
[13]O. Müller, J. P. Urbach, E. Goering, T. Weber, R. Barth, H. Schuler, M. Klemm, S. Horn, and M. L. denBoer, "Spectroscopy of metallic and insulating V_2O_3," Phys. Rev. B **56**, 15056 (1997).

[14]J.-H. Park, L. H. Tjeng, A. Tanaka, J. W. Allen, C. T. Chen, P. Metcalf, J. M. Honig, F. M. F. de Groot, and G. A. Sawatzky, "Spin and orbital occupation and phase transitions in V_2O_3," Phys. Rev. B **61**, 11506 (2000).
[15]F. Mila, R. Shiina, F.-C. Zhang, A. Joshi, M. Ma, V. Anisimov, and T. M. Rice, "Orbitally degenerate Spin-1 model for insulating V_2O_3," Phys. Rev. Lett. **85**, 1714 (2000).
[16]R. Shiina, F. Mila, F.-C. Zhang, and T. M. Rice, "Atomic spin, molecular orbitals, and anomalous antiferromagnetism in insulating V_2O_3," Phys. Rev. B **63**, 144422 (2001).
[17]S. Klimm, M. Herz, R. Horny, G. Obermeier, M. Klemm, and S. Horn, "Second spin-density wave phase in metalllic $V_{2-y}O_3$ close to the metall-insulator transition," Phys. Rev. B **64**, 184435 (2001).
[18]P. Pfalzer, "Lokale strukturelle und elektronische Eigenschaften von V_2O_3 und ZnV_2O_4," Ph.D. dissertation (Universität Augsburg, 2004).
[19]P. Pfalzer, G. Obermeier, M. Klemm, S. Horn, and M. L. den Boer, "Structural precursor to the metal-insulator transition in V_2O_3," Phys. Rev. B **73**, 144106 (2006).
[20]C. Müller, A. A. Nateprov, G. Obermeier, M. Klemm, R. Tidecks, A. Wixforth, and S. Horn, "Surface acoustic wave investigations of the metal-to-insulator transition of V_2O_3 thin films on lithium niobate," J. Appl. Phys. **98**, 084111 (2005).
[21]C. Müller, A. A. Nateprov, M. Klemm, A. Wixforth, R. Tidecks, and S. Horn, "Early stages of the metal-to-insulator transition of a thin V_2O_3 film," J. Appl. Phys. **103**, 063705 (2008).
[22]C. Müller, A. Nateprov, G. Obermeier, M. Klemm, V. Tsurkan, A. Wixforth, R.Tidecks, and S.Horn, "Surface acoustic wave devices, zinc oxide materials and devices II," Proc. SPIE **6474**, 647415 (2007).
[23]S. Hassan, A. Georges, and H. R. Krishnamurthy, "Sound velocity anomaly at the Mott transition: Application to organic conductors and V_2O_3," Phys. Rev. Lett. **94**, 036402 (2005).
[24]Md. Motin Seikh, C. Narayana, A. K. Sood, P. Murugavel, M. W. Kim, P. A. Metcalf, J. M. Honig, and C. N. R. Rao, "A Brillouin study of the temperature-dependence of the acoustic modes across the insulator-metal transitions in V_2O_3 and Cr-doped V_2O_3," Solid State Commun. **138**, 466 (2006).
[25]S. Populoh, P. Wzietek, R. Gohier, and P. Metcalf, "Lattice softening effects at the Mott critical point of Cr-doped V_2O_3," Phys. Rev. B. **84**, 075158 (2011).
[26]N. Kuroda and H. Y. Fan, "Raman scattering and phase transitions of V_2O_3," Phys. Rev. B **16**, 5003 (1977).
[27]W. Finger and R. M. Hazen, "Crystal structure and isothermal compression of Fe_2O_3, Cr_2O_3, and V_2O_3 to 50 kbars," J. Appl. Phys. **51**, 5362 (1980).
[28]H. Schuler, "Herstellung und Untersuchung epitaktischer V_2O_3 und Cr_2O_3 Schichten auf (0001) Saphir," Ph.D. dissertation (Universität Augsburg, 1997).
[29]H. Schuler, S. Klimm, G. Weissmann, C. Renner, and S. Horn, "Influence of strain on the electronic properties of epitaxial V_2O_3 thin films," Thin Solid Films **299**, 119 (1997).
[30]F. Simmet, "Transportmessungen an c-Achsen orientierten V_2O_3-Filmen," Diploma thesis (Universität Augsburg, 1995).
[31]A. Stierle and H. Zabel, "Kinetics of Cr_2O_3 growth during the oxidation of Cr(110)," Europhys. Lett. **37**, 365 (1997).
[32]A. Nateprov, "Investigation of growth, structural and electronic properties of V_2O_3 thin films on selected substrates," Ph.D. dissertation (Universität Augsburg, 2006).
[33]Z. Liu, "Metall-Isolator-Übergang in V_2O_3 Dünnschichten auf $LiNbO_3$-Substraten mit Cr/Cr_2O_3 Zwischenlagen," Diploma thesis (Universität Augsburg, 2008).
[34]P. Pontiller, "Charakterisierung des Metall-Isolator Übergangs von V_2O_3 mit akustischen Oberflächenwellen," Master thesis (Universität Augsburg, 2009).
[35]G. Kovacs, M. Anhorn, H. E. Engan, G. Visintini, and C. C. W. Ruppel, "Improved material constants for $LiNbO_3$ and $LiTaO_3$," Ultrason. Symp. Proc. **1990**, 435.